AIAA 95 3067

Plume Characteristics of a Multiple Source Ion Thruster

C. Michael Tierney*, John K. Brophy**, Juergen Mueller***
Jet Propulsion Laboratory
California Institute of Technology
Pasadena, California

This paper summarizes a description of several plume characteristics of the multi-ion source, segmented ion thruster (SIT) that rue important to propulsion subsystem, spacecraft system, and mission design engineers with respect to incorporation of inn thrusters within a space mission. These characteristics will address issues related to operational performance, lifetime, thruster interaction with a host spacecraft, multiple ion beam interaction, and repeatability of construction and operation.

Characteristics of the exhausted ion beam(s) were evaluated through two sets of experiments. The first involved measuring the two-dimensional ion current density distribution as a function of position downstream of the thruster with concurrent operation of up to three ion sources. Ion beam asymmetries about the ion source centerline were observed. Construction of multiple ion source current density profiles through superposition of data obtained from operation of individual ions sources appear to give the correct results provided the effects of charge-exchange collisions are accounted for. Beam divergence angles for cases in which the net-to-total accelerating voltage (R) was equal to 0.893 ranged from 10° to 18° and from 16° to 22° for those in which R = 0.643.

The second set of experiments involved collection of ion charge state data with the use of an ExB mass spectrometer placed downstream of the thruster. Measured double inn fractions were typically less than 10% except at very high propellant efficiencies.

Nomenclature

X: Horizontal Axis (m)
Y: Vertical Axis (m)
Z: Downstream Axis (m)
J_B: Metered Beam Current (mA)
V_S: Screen Voltage (V)
V_A: Accelerator Voltage (V)
V_D: Decelerator Voltage (V)
K: Net-to-Total Voltage Ratio
J_C: Collected Current (A)
J_E: Measured Beam Current (A)
m_t: Total Mass Flow Rate (seem)

Introduction

The primary objective of this effort was to assist in the development of the segmented ion f.brusher (SIT) [1]. The information contained in this paper is a summary of the results presented by Tierney [2,3] which describes two types of experiments [0 characterize the S["1" exhaust plume: Faraday probe current density and Ex B mass spectrometer ion charge state. These results could be used by propulsion subsystem, spacecraft system nnd mission design engineers in order to assess the benefits, risks, and costs associated with incorporating the SIT with a given spacecraft and mission. In addition, these results could be used in order to assess issues regarding thruster performance, lifetime, interaction with the spacecraft, interaction between multiple ion beams, and repeatability of ion source construction and operation.

km propulsion has been under development for over 30 years and been proposed for application as auxiliary propulsion for orbit raising and station keeping of earth orbiting satellites [4] and as primary propulsion for deep space and planetary exploration platforms [5,6,7,8,9]. It has also been proposed for use in the operation of large space systems that could have an extensive set of earth orbiting and planetary missions [10]. The segmented ion thruster (SIT) has also been suggested for application to several solar system exploration missions [11, 12]. Shown in Fig. 1, the segmented ion thruster consists of four separate ion sources, each with its own 3-grid accelerator system.

Production of multiply charged ions within the discharge chamber of an ion thruster degrades the ideal performance of the thruster and increases internal erosion rates. In this investigation the charge state of the accelerated ions was measured along the centerline of a single segment in order m assess the degradation of performance and life as a function of

* Graduate Student, Department of Aeronautics, California Institute of Technology
** Supervisor, Advanced Propulsion Technology Group, JPL
*** Member of the Technical Staff, Advanced Propulsion Technology Group, JPL.

the ion source berm current (J_B). This was accomplished by placing an ExB mass spectrometer downstream of the operating segment and measuring the collected current (J_c) as a function of voltage applied to the deflector plates.

Lifetime of an ion thruster is primarily limited by erosion of the accelerator system grids duc to sputtering of grid material by charge exchange ions,

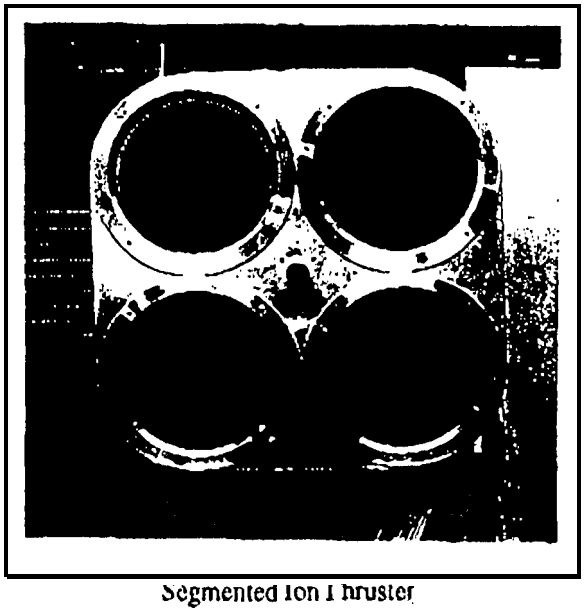

Segmented Ion Thruster
Figure 1

The two ion beam characteristics evaluated in this investigation that impact lifetime were beam uniformity rind multiply charged ion production. Maximum grid lifetime is achieved with uniform, flat beams with production of only singly charged ions. A non-uniform or non-flat beam profile will produce uneven erosion of the grid material and therefore accelerate the erosion rate in some regions compared to that of the ideal case.

Divergence of the extracted ion beams can be described by the beam divergence angle (α) arrd help identify "keep out" regions for solar arrays and other spacecraft appendages in order to prevent direct ion impingement on spacecraft surfaces, 'his angle is defined as the half cone angle measured from the edge of the active ion source, which contains 95% of the beam current. Due [0 charge exchange effects, the measurable beam current (J_z) tends to decrease as a function of distance from the thruster (2), The beam divergence angle *(a)* was calculated for each plane of Faraday probe current density data collected during the individual operation of each ion source,.

The primary design feature of the segmented ion thruster which makes it different from other ion thrusters is the tour ion source configuration. In order to study the operation of multiple ion sources, this investigation will compare the beam current density profiles generated from multiple ion source operation to the equivalent profiles created mathematically through superposition of the data obtained from operation of single sources.

Apparatus

Test Facilities

Testing was conducted in a 2.4 m-dia. x 5 m long stainless steel vacuum facility with an effective pumping speed on Xe of -14,000 L/s. A more detailed description of the facility and SIT support hardware is given by Mueller et al.[13].

Segmented Ion Thruster

The segmented ion thruster shown in Fig.1 is made up of four 15-cm diameter ion sources of the type described by Brophy et al. [14]. Each ion source is n modified, scaled-down version of the NASA light-weight, 30-cm diameter ring-cusp thruster [15]. Each discharge chamber body is made of 6061 aluminum and the ring-cusp magnetic field configuration is formed from two rings of samarium-cobalt magnets; one positioned at the upstream end near the. cathode and the other at rhc downstream end near the accelerator system. Two of the ion sources have the polarity of their magnet rings reversed to give a right and left-handedness to the sources, In the SIT configuration, the ion sources are integrated such that segments A and C are right-handed and B and D are left-handed.

The ion source segments are integrated onto a base plate structure at ground potential. Electrical insulators between the segments and to the centrally located neutralizer assembly are used to make the overall structure rigid. Each ion source is electrically isolated from the others. Electrical integration of the ion source segments is accomplished at the power supplies. This enables a faulty ion source to be isolated from the others, A single, centrally-located neutralizer cathode is used to neutralize all of the ions sources. For a flight propulsion system which consists of a single SIT, a second neutralizer cathode would likely be included for redundancy.

Three sets of 3-grid ion accelerator systems were fabricated from carbon-carbon. A fourth set was damaged during fabrication srnd could not be used. Ion source segments A, B and C were equipped with the carbon-carbon grids, Difficulties in operation of segment D precluded use of this segment for data acquisition. Geometries of the carbon-carbon grids, sss well as derails of the fabrication and operation are summarized by Mueller et al. (16].

Probes

Two different types of charged particle probes were used in this investigation, Faraday probes and an ExB mass spectrometer. A total of 24 Faraday probes were mounted to a vertical rake with 5 cm between probe centers. Shown in Fig. 2, the button portion of each probe was 2,3 cm in diameter with a -0.1 cm thick tungsten coating on the surface to reduce secondary electron emission. The cup and button were biased -30 V with respect to the surrounding tank wall in order to repel free electrons within the ion beam.

The ExB mass spectrometer, shown in Fig. 3, consists of a fixed magnetic field in the vertical direction and, through the use of a programmable power supply, has a variable electric field in the horizontal direction. The collector surface is also covered with -0.1 cm thick layer of tungsten for reduction of secondary electron emission,

Probe Positioning System

Both the Faraday probe rake and the ExB mass spectrometer were separately mounted to a 3 axis probe positioning system. This system uses recirculating ball bearing pillow blocks, stainless steel slide rails, recirculating ball screws and stepper motors for motion actuation. Motion of the system was controlled by a Macintosh Centris 650 computer with LabView software, a digital I/O card, and stepper motor drive electronics. In order to determine the position of the traverse mechanism wish respect to a predefined origin, the LabView software counts the number of TTL pulses transmitted to the stepper motor drive electronics, and knowing the lead of the ball screws, the computer calculates the location.

The coordinate axes of the probe positioning system are as follows: looking downstream from the point of view of the SIT, X axis - Left/Right, Y axis - Up/Down, Z axis - Front/Back. The origin of these axes correspond m X,Y,Z = 0.0,0 and is located in the lower left hand corner of the tank with the Faraday probe collector surfaces at the thruster exit plane. Positive x travel is from left to right, positive Y travel is from bottom to top, and positive Z travel is from upstream to downstream.

Data Acquisition Systems

Two different data acquisition systems were used, one for Faraday probe data collection, and another for ExB probe data collection. The Faraday cups were each connected across resistors through a bias power supply to ground. A voltage conversion modu le converted the voltage drop read across a resistor (±50 mV range) to a signal (± 5 V range) which could be read by an analog I/O board wi thin the Macintosh computer, The same LabView program used to control motion of the probe positioning system was also used to collect the Faraday probe data. Due to the number of Faraday probes used and the limited number of channels available on the 1/0 board, a multiplexer was used.

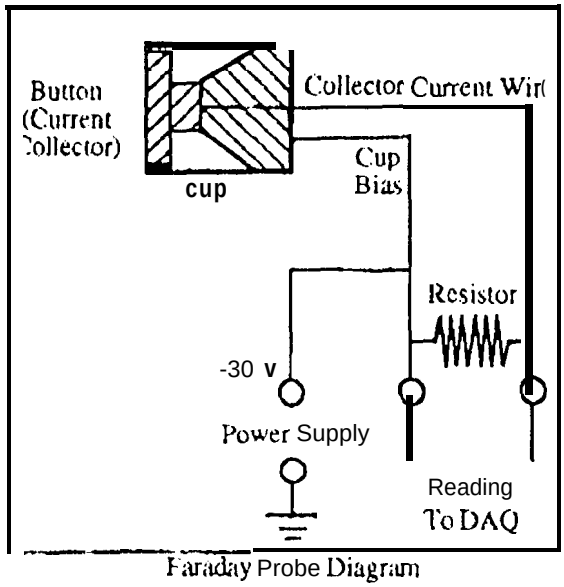

Faraday Probe Diagram
Figure 2

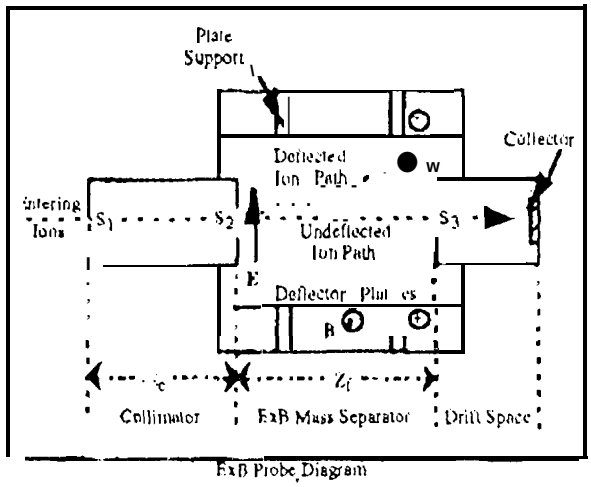

ExB Probe Diagram
Figure 3

The ExB probe data acquisition system consisted primarily of a Keithly 617 Electrometer which was used in measure the current collected by the ExB probe for a given potential difference across the probe's deflector plates. The measured value was then dig i tally transmitted to the Macintosh computer via a GPIB interface.

Faraday Probe Current Density Experiment

Thruster Operation

Al l combinations of segments A, B, and C were operated at three different beam currents and two different net-to-total accelerating voltages ratios (R). Table 1 gives each of these operating conditions.

Table 1

Data Set	I_B (mA)	V_S (v)	V_A (V)	V_D (V)	R
1	430	1250	-150	-100	0.893
2	312	1250	-150	-100	0.893
3	500	1250	-150	-100	0.893
4	430	900	-500	-200	0.430

Operating Conditions

Data Collection

Faraday probe data was collected at a total of 5 downstream location (Z = 0.356,0,508,0.660,0,813, 0.965 m) for data set 1 and a total of 3 downstream locations (Z= 0.356, 0.660.0.965 m) for data sets 2, 3, nnd 4. At each of these downstream positions, the Faraday probe rake was moved back and fourth through the ion beam(s), stopping every 2.54 cm, and collecting a total of 100 samples for each probe at each position. Each set Of 100 samples was averaged and the standard deviation was computed.

Data Adjustment and Reduction

Several adjustments to the raw data were required in order to account for non-ideal operating conditions of the experiment, prepare the collected data for analysis, rind to transform the data into a more presentable form. These adjustments included: removal of data collected during thruster recycle events; formation of the data into 2-D matrices; removal of biases believed to be caused by non-zero pressures within the vacuum facility; accounting for secondary electron emission; conversion to metric units; conversion of measured currents to current densities for a given probe collector area; construction of superimposed, multiple ion source data; and interpolation of 2,54 cm spaced data to produce 0.635 cm spaced values.

Data Analyses

Current density contour plots were constructed for all combinations of operating segment(s), ion source operating condition, and downstream location of the Faraday probe data acquisition plane. A 2-dimensional Simpson's Rule was applied to the data matrices in order to calculate the total measured downstream beam current. Reduction in the measured beam current compared to r-he metered beam current was expected due to charge exchange effects and comparisons between the measured and expected beam currents were made. Using the 0.635 cm spaced values for single ion source operation, the beam divergence angles were calculated.

Beam Symmetry Evaluation

Figures 4, 5, and 6 depict typical current density contour plots for the ion beams extracted from segments A, B, rind C respectively, The plots were generated from darn collected 0.660 m from the thruster a metered beam current (J_B) of 430 mA and R = 0.893. The step size between unlabeled contours is equal to the maximum labeled contour. One observable characteristic Of these contours is they are not round, but elliptical in shape. Similar investigations into the characteristics of other ion thruster plumes generally present results of uniform beams, such as in the work done by Feam et al. [17] and Groh et al. [18]. In addition, the degree to which each segment produces non-uniform beams is different as is the orientation of the beam profiles. Orientation of the ion beam profiles can be described by using the vertical axis (Y) through the center of an ion beam with the 12 o'clock position being *zero* rotation, measuring positive rotation in a clockwise direction from that position.

As shown in Figs. 4 through 6, the ion benm extracted from segment A appears to be the most asymmetric in comparison to those from segments B and C. The segment A "semi-major axis" is canted about +15°. Segment B seems to produce the least asymmetric beam and the "semi-major axis" lies at approximately 90°. With an orientation of close [0 0°, the beam extracted from segment C appears closer to segments A with respect to the degree of asymmetry.

The most likely cause for non-uniform beam profiles involves misalignment between the grid holes of the accelerator system. Alignment of these holes affects the trajectories of the accelerated ions, If all holes of adjacent grids are not radially consistent in alignment. the ions will exit in such a manner that the resulting current density profile will not be symmetric. Variable spacing between the grids, position errors in drilling of the holes, inexact assembly of the grids, and variations in thermal expansion of the grids are all potential factors in hole misalignment. Variations in spacing between the grids could be caused by differences in spacer thickness or by non-flatness of the grids.

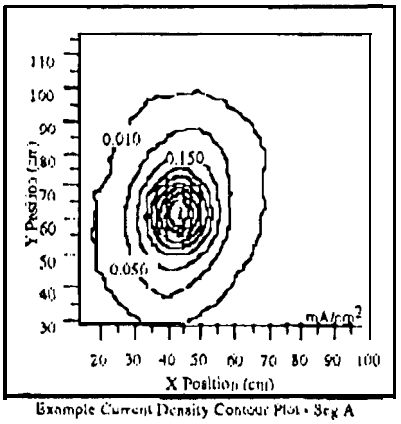

Example Current Density Contour Plot - Seg A

Figure 4

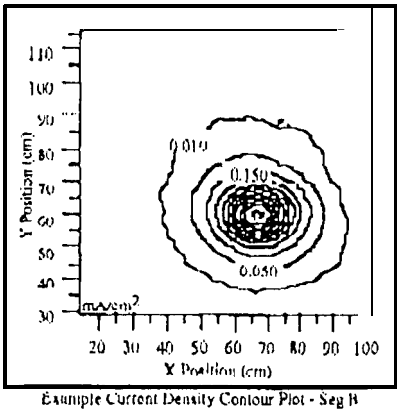

Example Current Density Contour Plot - Seg B

Figure 5

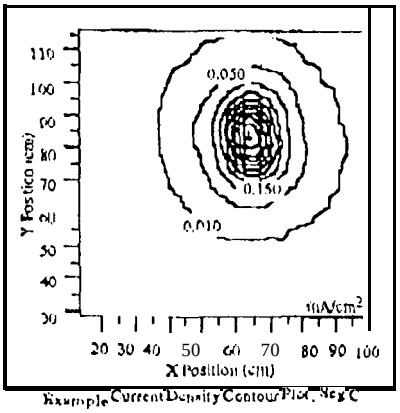

Example Current Density Contour Plot - Seg C

Figure 6

Downstream Beam Development

Figures 7 m 9 display example current density contour plots at three different downstream locations. The data used to create Fig. 7 was acquired at a distance of 0.356 m from the ion exit plane of the thruster with data for Figs. 8 and 9 collected at 0.660 m and 0.965 m respectively. Each ion source had u metered beam current of 430 mA and an K ratio of 0.893 with a screen voltage (V_S) of 1250 V.

As distance from the thruster increases, the beam tends to spread and the peak current density decreases. The 0.050 and 0.175 mA/cm2 contours do not appear to increase in size significantly and seem to retain the initial shape. The 0.010 mA/cm2 Contour however, does cover a greater area with distance from the thruster. This beam development is primarily due to divergence of the individual ion beamlets extracted from each hole of the accelerator system.

Real vs. Superimposed Current Density Contour Plots

The general shape, orientation, and location of the superimposed current density contour plots agree well in comparison to the current density plots generated with data acquired from the actual operation of multiple ion sources. Figures 10 through 13 depict four sample comparisons. In cases where Faraday probe data was collected at positions close to the thruster there is little discrepancy between real nnd superimposed contour plots (Figs. 10 and 11). However, as distance from the thruster increases, the differences become more pronounced. These differences refry indicate interaction between the ion beams, however, this interaction more likely is due to facility and resulting charge exchange effects. The differences between Figs. 12 and 13 are much more pronounced than those between Figs. 10 and 11. The only difference in the operating conditions between Fig. 120 and Fig. 12 is the number of active ion sources, 3 for Fig. 12 and 2 for Fig. 10. Addition of an active ion source in Fig 12 would have increased the facility pressure compared to that found in Fig. 10 due to the higher propellant flow rate, and therefore increased the charge exchange effects on the ion beams.

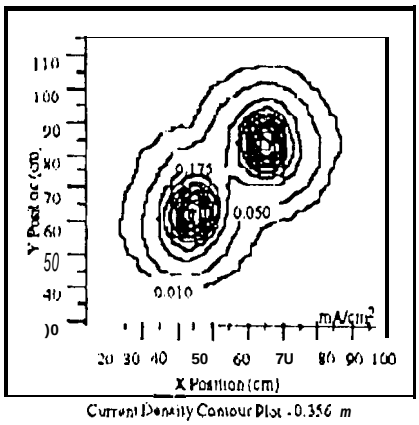

Current Density Contour Plot - 0.356 m
Figure 7

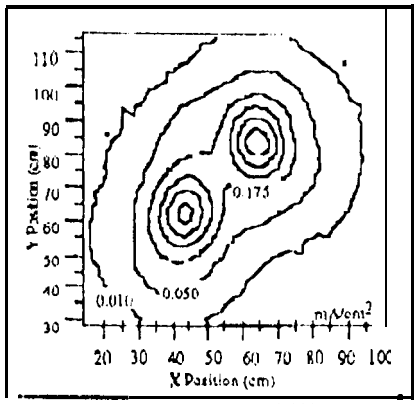

Current Density Contour Plot -0,660 m
Figure 8

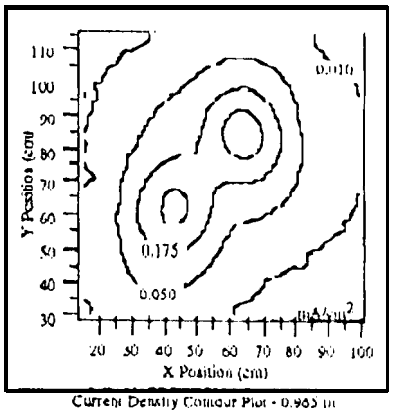

Current Density Contour Plot - 0.965 m
Figure 9

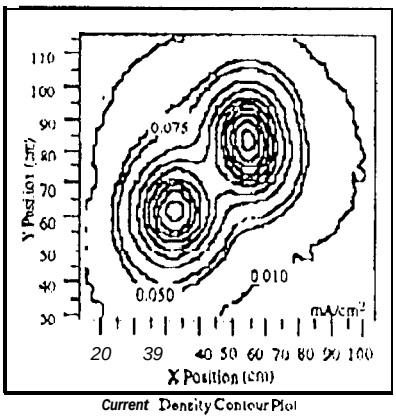

Current Density Contour Plot
Real Data . Z . 0.965 m
Figure 10

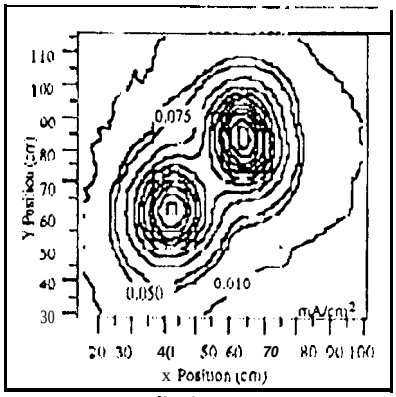

Current Density Contour Plot
Syn I-)411. Z = 11,96>,11
Figure 11

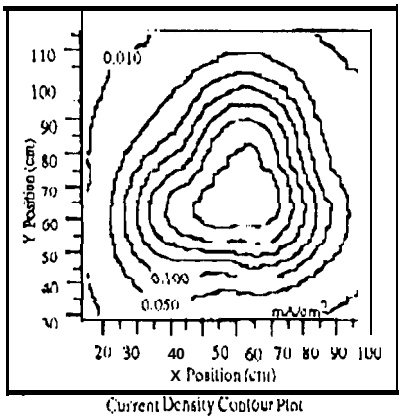

Current Density Contour Plot
Real Data Z = 0.965 m
Figure 12

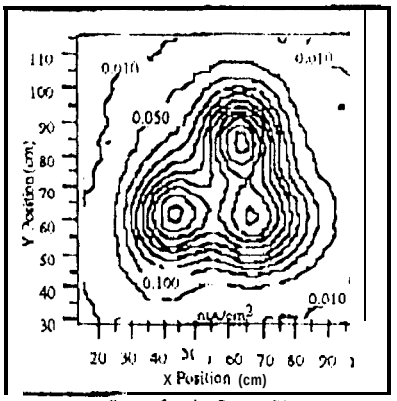

Current Density Contour Plot
SynData - Z = 0.965 m
Figure 13

Measured vs. Calculated Beam Current

Most of the discrepancies between the integrated (measured) beam currents and the theoretically calculated beam currents based on charge exchange effects were less than 10% for cases in which R = 0.893, The range was as high as 20% and as low as 2%. However, for cases in which R = 0.643, the discrepancies were rarely less than 15%, with some as high as 28%. In a total of 66 out of the 83 with R = 0.893, the uncertainties associated with the theoretical and integrated beam currents could account for the discrepancies between the values. This agreement between the calculated and measured values does not hold well for cases where R = 0.643. Only 1 of the 21 cases could account for the differences. This level of disagreement between the measured and calculated values was unexpected and attempts were made to better understand this.

Attention was focused on the assumptions used to account for charge exchange effects. One of the assumptions used in the theory was that of a highly collimated beam. With a lower R ratio for these cases, the ion beam tended to be wider than for a higher R ratio. The charge exchange calculations used the axial distance between the probes and the thruster exit plane, which were fixed at 0.356, 0.506, 0.660, 0,813 or 0.965 m. It would have been more appropriate m use the distance between the center of the thruster at the ion exit plane and each individual probe, as opposed to the normal distance to the data acquisition plane. This would have accounted for the physical distance the ions traveled Although using this off axis distance would have been more accurate, iris not feasible to determine where on the exit plane of the multiple ion sources would be the appropriate spot from which to measure.

Superimposed vs. Measured Beam Current

Comparison of the beam current values integrated using measured and superimposed data values showed that the integrated beam currents using superimposed data were generally greater than those using measured data. The differences were normally less than 8% with Some exceptions. Differences in 40 of the 56 cases could be accounted for by evaluating the uncertainties associated with both integrated values. There seemed to be some dependence of these differences on the number of active ion sources. The discrepancies tended to be higher for cases in which three. ion sources were operating. This could have been related to either the interaction 01 ion beams or there may have been a facility effect that was dependent upon the xenon mass flow rate and pumping speed. There did not appear to be any dependence of this on R ratio, ion source beam current, or distance from the thruster.

Beam Divergence

Beam divergence angles (α) tended to vary between segments and were dependent upon the metered beam current and R ratio. Al though the measured divergence angle varied with downstream position, no trend was identified.

Figures 14 through 16 display the beam divergence angles for each segment at the different operating conditions. Segment B tended to produce the most collimated beam among the three segments. Segments A and C traded positions for having the most divergent plumes as metered beam current and R varied. The available beam divergence angles were averaged along with (heir associated uncertainties in order [o enable a quantitative comparison of the results between the different thruster operating conditions as given in Table 2.

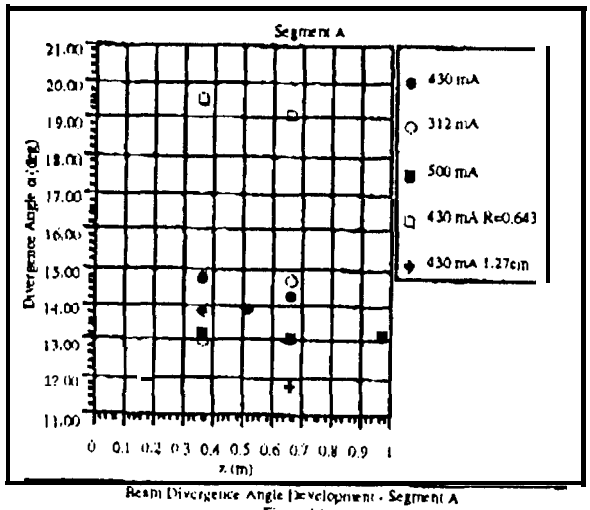

Beam Divergence Angle Development - Segment A
Figure 14

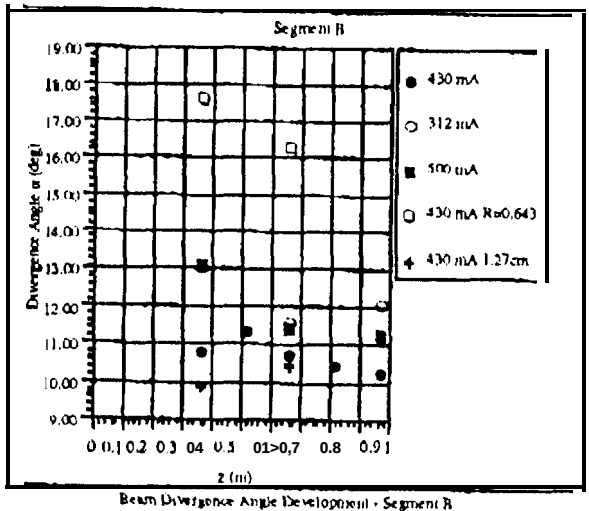

Beam Divergence Angle Development - Segment B
Figure 15

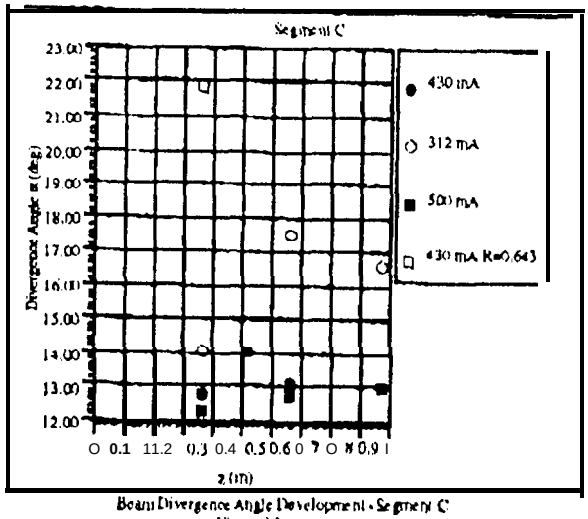

Beam Divergence Angle Development - Segment C
Figure 16

The most dramatic shift in beam divergence angle (α) occurs when the R ratio changes from 0.893 to 0.643. The width of the ion beams emanating from each of the segments increase 34, 56, and 63 percent for segments A, B, and C when compared to the beams produced with the thruster operating at 430 mA with R = 0.893. This increase in beam divergence has been identified as a possible cause for R = 0.643 integrated beam current values to be cm the order of 20% lower than the beam current values expected after accounting for charge exchange effects. A huge change in α is also visible between segment C at 312 mA and 430 mA or 500 mA.

Table 2

Segment	I_B (mA)	R	α (deg)	dα (deg)
A	430	0.893	14.7	0.4
B	430	0.893	11.0	0.3
C	430	0.893	13.6	0.4
A	312	0.893	14.2	0.5
B	312	0.893	12.1	0,4
C	312	0.893	16.4	1.2
A	500	0.893	13.5	0.3
B	500	0.893	22.2	0.3
C	500	0.893	13.0	0.3
A	430	0.643	19.7	0.9
B	430	0.643	17.2	0.9
C	430	0.643	22.2	1,2

Average Beam Divergence Angle Results

ExB Probe Charge State Experiment

Thruster Operation

only segment A was used for this portion of the investigation. For the centerline data collection part Of this experiment, three nominal beam currents were used, 312 mA, 430 mA, and 470 mA. The corresponding propellant flow rates ($\dot{m}_1$) were set such that an uncorrected propellant utilization efficiency of 0.90 would be produced (4.83, 6.66, 7.27 seem). Once the propellant flow rate was set, the discharge current was ramped, both in the positive and negative directions, such that the uncorrected propellant utilization efficiency would range from about 0,50 up to over 1,10,

For the radial profile data collection portion, the beam current and propellant flow rate were fixed at 430 mA and 6.66 seem, respectively,

Data Collection

The ExB mass spectrometer was initially positioned 0.61 m downstream of the thruster with the centerline of the collimator approximately along [he segment A centerline, For the centerline

experiment, the probe remained at that position for all data collection. The probe was translated along the horizontal and vertical axes. one at a time, in 0.635 cm increments. Data was collected at each location. The range of motion along both axes was sufficient such that at the limits, no singly or doubly charged ion signals were detected.

Data Adjustment and Reduction

Similar adjustments were made to the ExB data in order to account for facility background pressures. The collected data was also smoothed in order to more easily determine peak values and adjustments were made to the propellant utilization c. fficiency values to account for propellant backflow into the discharge chamber.

Data Analyses

Several analyses were performed with the adjusted data previously described. Collected current (I_C) vs. deflector plate bias were plotted in order to determine the measured peak singly and doubly charged ion currents. The charge state current (R_c) and number (R_n) ratios were calculated, propellant utilization efficiencies corrected for doubly charged ion production and propellant mass ingestion were calculated, charge state thrust correction factors were calcu lated, and plots of η_p vs. R_n and f_c vs. R_n were developed. Propellant utilization e fficiency (η_{pc2}) uncertainty analyses were also conducted.

Centerline Charge State Data Plots

Ion beam centerline charge state was evaluated for a total of five different thruster operating conditions. These conditions correspond to nominal beam currents of 312 mA, 430 mA, and 470 mA. Nominal beam current refers to the metered beam current at which the uncorrected propellant utilization efficiency (η_p) is 0.90.

Data generated from these measurements are presented in charge state number ratio (R_n) vs. corrected propellant utilization efficiency (η_{pc2}) plots given in Fig. 17 through 21. Error bars are included in the plots to show uncertainties in the calculation of η_{pc2}.

A significant aspect of these curves is that the corrected propellant utilization efficiency is still greater than 1 for beam currents greater than about 370 mA. Since this is physically impossible, attempts were made to explain this regarding uncertainty in measuring doubly charged ion production and discharge chamber propellant ingestion. For [he data points in which η_{pc2} is greater than 1. the associated error bars extend over the η_{pc2} - 1 line for all but one case, which means that only one data point may be truly suspect. This data point of η_{pc2} - 1.05, shown in figure 19, corresponds to thruster operating conditions of I_B = 425 mA, $\dot{m}_t$ = 4.85 sccm, and V_{DIS} = 49.1 V.

Initially in this investigation it was assumed that production of triply charged ions could be neglected. According to Sovey [19], production of triply charged ions did not begin until the discharge voltage reached approximately 42 V. The reason it was assumed that triply charged ion production would be negligible was because reaching discharge voltages of over 40 V was not anticipated. Sovey found that at discharge voltages of 46 V the triply charged ion production rare was 2% of the singly charged ions. If triply charged ions were produced at these higher discharge voltages in this investigation, then the propellant utilization efficiency corrected for doubly and reply charged ions as well as propellant ingestion would be 1.041 ± 0.046. Note here that the uncertainty would allow the error bars to extend over the η_{pc2} = 1 line and account for the greater than 1 value.

Charge State Thrust Correction Factor

Figures 22 through 26 display the ion beam charge state thrust correction factors (f_c) as a IuIIC11OI) of beam current for given propellant flow rates.

Radial Charge State Ratio Plots

Figures 27, 28, 30, and 31 display the collected current radial profiles for singly (I^+) and doubly (I^{++}) charged ions generated by segment A. These profiles were created with measurements from an ExB mass spectrometer probe, which was located ().61 m downstream or the thruster. Figures 29 and 32 show the resulting charge state number ratio (R_n) radial profiles. Some unexpected characteristics of the radial profiles resulted, however, and there was insufficient data to assess repeatability of the results.

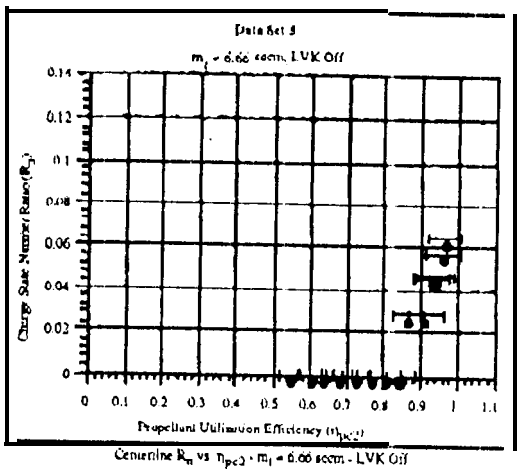

Centerline R_n vs. η_{pc2} - m_i = 6.66 sccm - LVK Off
Figure 17

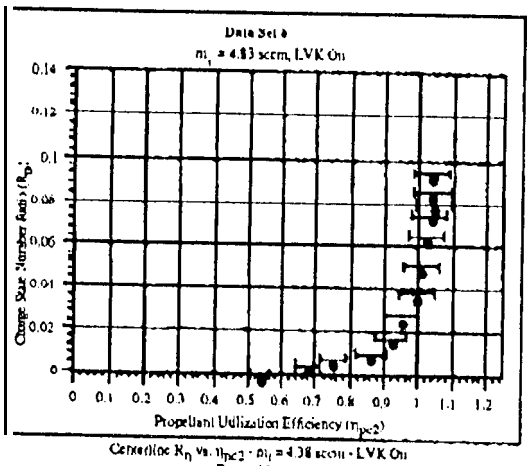

Centerline R_n vs. η_{pc2} - m_i = 4.83 sccm - LVK On
Figure 18

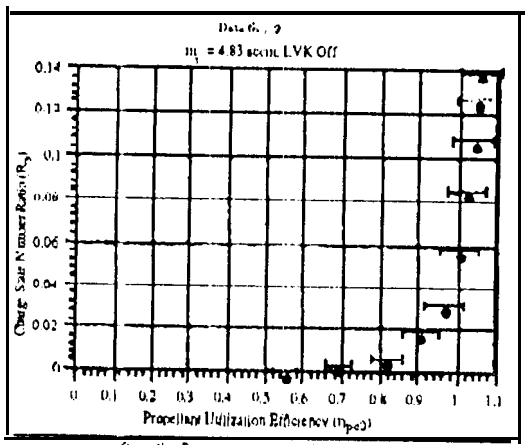

Centerline R_n vs. η_{pc2} - m_i = 4.83 sccm - LVK Off
Figure 19

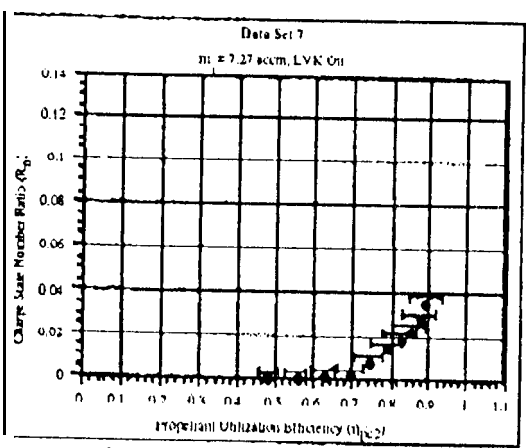

Centerline R_n vs. η_{pc2} - m_i = 7.27 sccm - LVK On
Figure 20

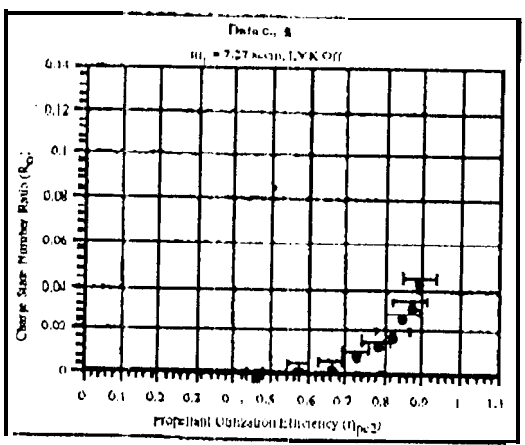

Centerline R_n vs. η_{pc2} - m_i = 7.27 sccm - LVK Off
Figure 21

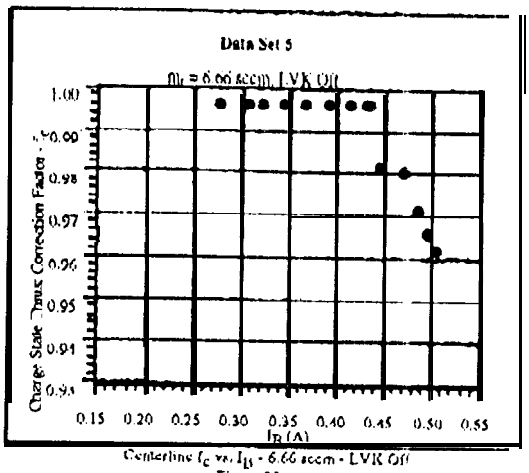

Centerline f_c vs. I_B - 6.66 sccm - LVK Off
Figure 22

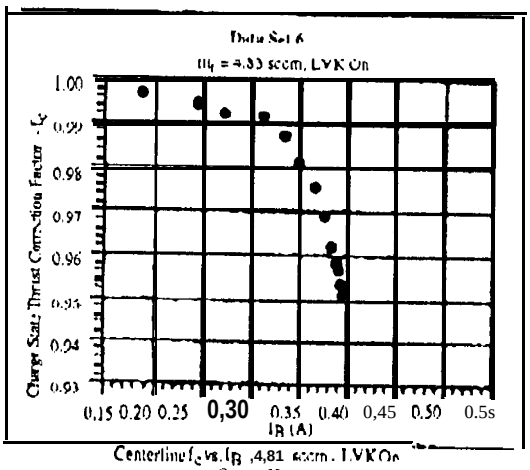

Centerline f_c vs. I_B ,4.81 sccm - LVK On
Figure 23

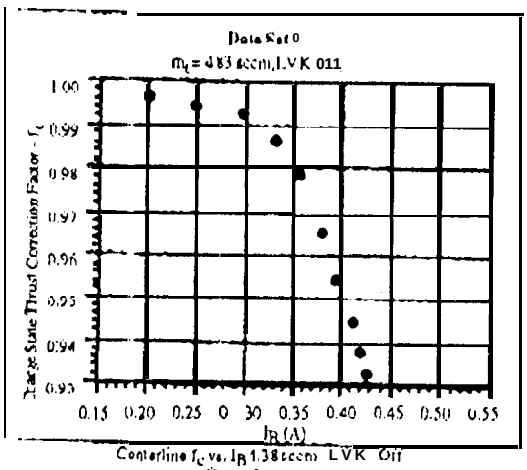

Centerline f_c vs. I_B 4.38 sccm LVK Off
Figure 24

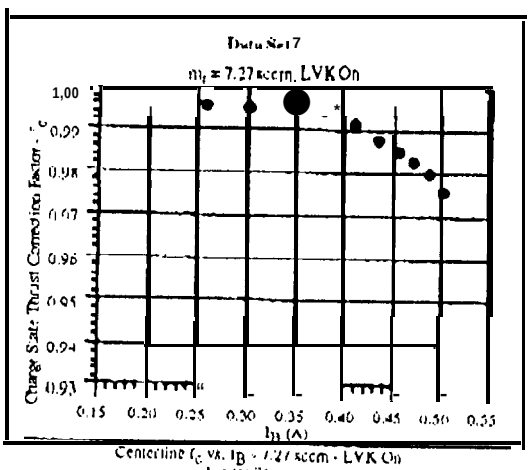

Centerline f_c vs. I_B - 7.27 sccm - LVK On
Figure 25

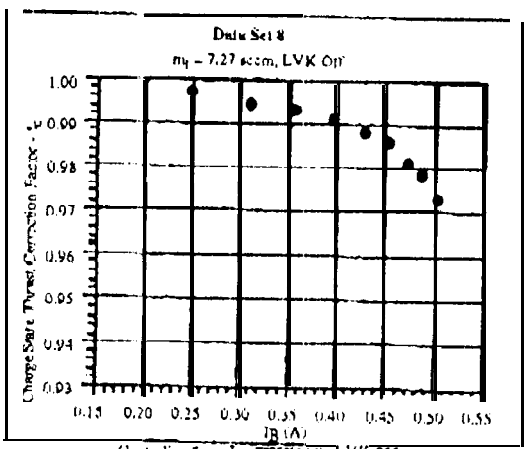

Centerline f_c vs. I_B - 7.21 sccm - LVK 011
Figure 26

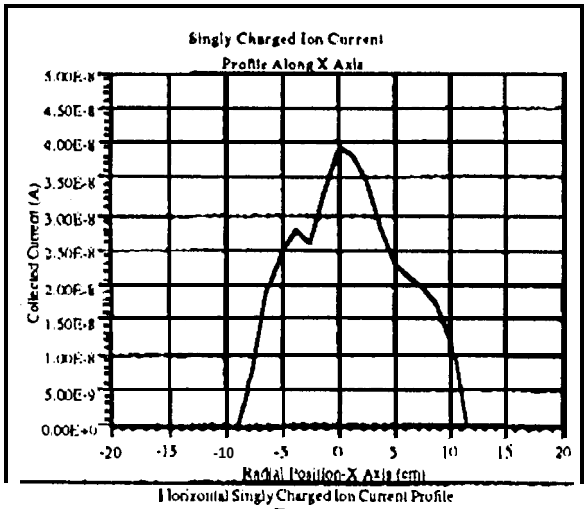

Horizontal Singly Charged Ion Current Profile
Figure 27

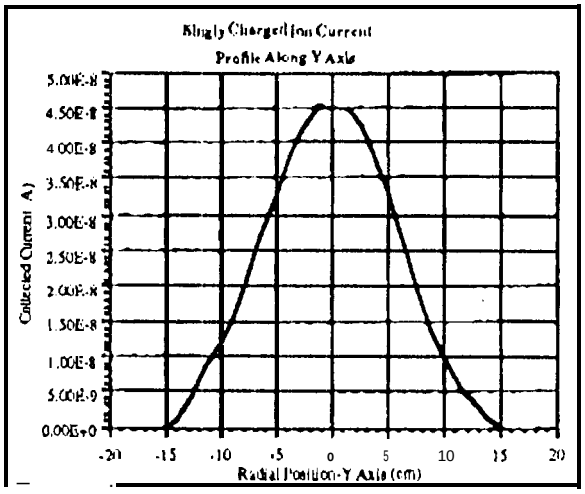

Vertical Singly Charged Ion Current Profile
Figure 30

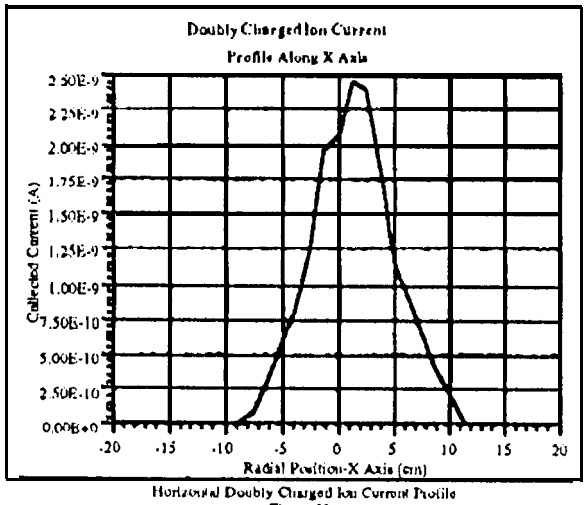

Horizontal Doubly Charged Ion Current Profile
Figure 28

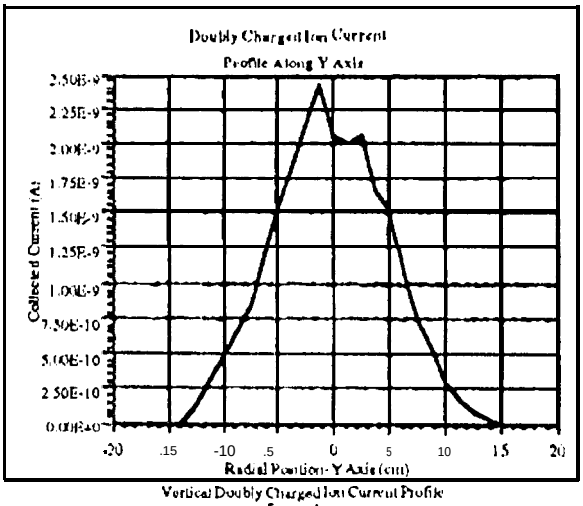

Vertical Doubly Charged Ion Current Profile
Figure 31

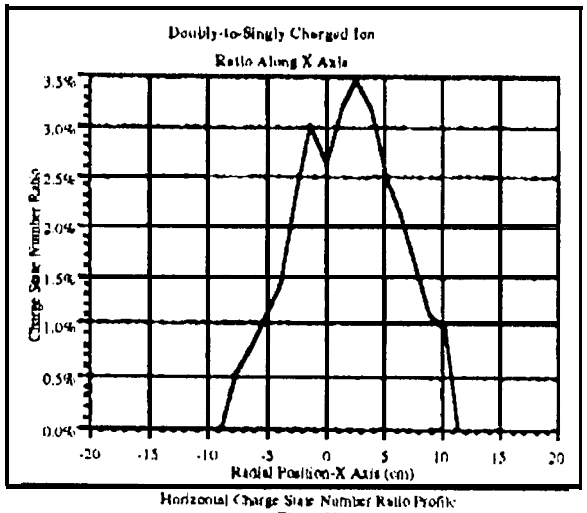

Horizontal Charge State Number Ratio Profile
Figure 29

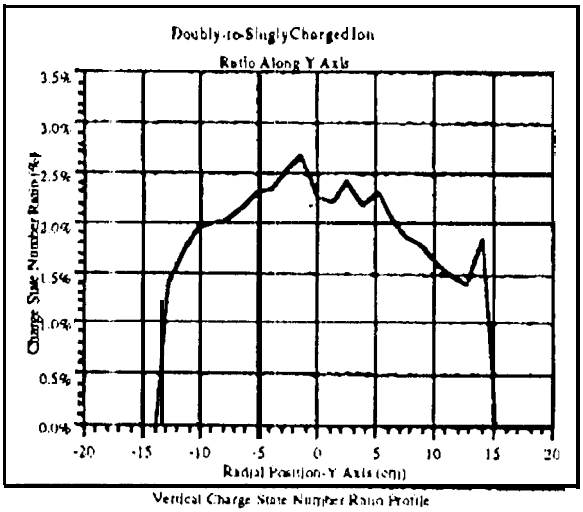

Vertical Charge State Number Ratio Profile
Figure 32

Conclusions

Performance

The charge state thrust correction factor (f_c) is given in figures 22 through 26 as a function of metered beam current (I_B) for three propellant flow rates. The values for f_c are based upon the measured charge state number ratio (R_n) along the centerline of the segment A discharge chamber. According to the R_n vs. X and Y plots given in figures 29 and 32, the maximum value for R_n is not located along the centerline, and therefore, these f_c values cannot be considered worst case. The worst case values, in reference to the R_n vs. X profiles, are between 17 and 30 percent larger than the centerline values.

The propellant utilization efficiency (η_{pc2}), corrected for doubly charged ion production, is given in figures 17 through 21 as a function of the centerline charge state number ratio (R_n) for the same three propellant flow rates used for determination of f_c. The η_{pc2} values given in these figures were also corrected for ingestion of propellant into the discharge chamber due to facility background pressure. Some of the η_{pc2} values given in figures 18 and 19 were greater than 1.0. In all but one of these cases, the uncertainty in the measurements was sufficiently large to account for the greater than 1 values. For the single case, shown in figure 19 at R_n = 0.14, in which the uncertainty could not account for the greater than 1 value, the production of triply charged ions is believed to be the cause.

Spacecraft Interactions

Direct ion impingement was the only interaction effect addressed in this report. So long as spacecraft components are not in the path of primary ions extracted from the thruster accelerator system, the potential for degradation try sputtering should be minimal. The divergence of the extracted ion beams from segments A, B and C for four different operating conditions of the thruster were evaluated. Beam divergence angles for R = 0.893 cases ranged from 10° to 16° and from 17° to 22° for cases in which R = 0.643. The beam divergence angle was generally greater for segment A than for either segments B or C. These values are presented in figures 14 through 16. Beam divergence appears to primarily be a function of R ratio and ion source and not of beam current or distance from the thruster.

Lifetime

The centerline double ion ratio tended to be less than 10% except for cases at very high propellant utilization efficiencies and never exceeded 5% for propellant efficiencies of less than 0.9. Although this is not ideal, the sputter erosion due to double ion production is expected to be low.

Interaction of Multiple Ion Beams

No substantial evidence was found to indicate that interaction between multiple ion beams occurred. Generally the consistency was strong between the current density contour plots generated with real and superimposed data. The differences observed, which could possibly have indicated beam interaction, may be explained by slight inconsistencies within the investigation to account for background plasma biases and charge exchange ion effects. Numerically integrated beam currents calculated with real mostly agreed with those calculated with superimposed data within the limits of uncertainty and those that did not could also be explained by background plasma bias and charge exchange effects.

Repeatability of Construction and Operation

Differences in the beam current density profiles observed for individual operation of each segment demonstrated some inconsistencies in construction or fabrication of the ion sources, accelerator systems, or the integration of the system. These differences were observed in both the shape of the individual ion beams as well as the orientation of the beams profiles with respect to the thruster. Due to some differences between the ion beam profiles measured in an early portion of Uris study and those presented here signify that the differences in the assembly of the ion optics is the most likely cause.

Future Work and Recommendations

The beam divergence! thrust correction factor (f_d) and the beam flatness parameter (F) measured close to the thruster were not investigated in this effort. Both of these ion beam parameters could be of value in the overall plume characterization. The data required to assess the beam divergence thrust correction factor is available, however, further experimentation would be required to collect current density data close to the thruster.

In the assessment of interaction between multiple ion beams it may have been possible to filter out the charge exchange effects that are believed to have been observed. This would facilitate a more appropriate comparison between the current density contour plots and integrated beam currents.

Large discrepancies exist between X and Y axis charge state number ratio profiles with regard to symmetry and profile shape. This was most likely